Realgar-induced KRAS mutation lung cancer cell death via KRAS/Raf/MAPK mediates ferroptosis

XIAOFENG LIU[1*], YANG HAI[3,5*], JINQU DONG[1], LAN XU[1], WENQIAN HOU[1], JING SU[1], WEIYU REN[1] and DONGLING LIU[1,2,4]

[1]School of Pharmacy, Gansu University of Chinese Medicine; [2]Gansu Provincial Key Laboratory of Pharmacology and Toxicology of TCM; [3]Scientific Research and Experimental Center, Gansu University of Chinese Medicine; [4]Northwest Collaborative Innovation Center for Traditional Chinese Medicine; [5]Research Center of Traditional Chinese Medicine, Lanzhou, Gansu 730000, P.R. China

Received July 14, 2022; Accepted October 13, 2022

DOI: 10.3892/ijo.2022.5447

Abstract. KRAS is a biomarker for non-small cell lung cancer-targeted therapy, but there is currently no effective KRAS-targeting medication. Realgar is an impelling anti-cancer drug, however its significance in KRAS mutant lung cancer is uncertain. According to our findings, the IC_{50} of H23 (KRAS mutant) cells is 2.99 times lower than that of H1650 (non-KRAS mutant) cells. Flow cytometry and the Hoechst 33258 staining assay revealed that H1650 cells treated with 4 μg/ml realgar had an apoptotic rate of 8.2%, while H23 cells had a rate of 21.46%. Accordingly, realgar was more sensitive to KRAS mutant cells. Transcriptome sequencing test indicated that there were 481 different expression genes in H23 cells treated with realgar. In H23 cells treated with realgar, mitochondria shrank, inner membrane folding was disturbed, and mitochondrial membrane potential crushed. Realgar boosted intracellular Fe^{2+}, reactive oxygen species, malondialdehyde and glutathione levels, which were all reversed by ferroptosis inhibitor Fer-1. Realgar decreased phosphorylated p-Raf, p-ERK1/2 and increased p-p38 and p-JNK, whereas only p-Raf was abolished by Fer-1. Raf inhibitor Sorafenib accelerated the realgar-induced ferroptosis. On H23 cells treated with realgar, the expression of GPX4, SCL7A11 decreased while ACSL4 expression increased; this effect could also be amplified by Sorafenib. In conclusion, the present study indicated that realgar may induce ferroptosis by regulating the Raf, and hence plays a role in anti-KRAS mutant lung cancer.

Introduction

Lung cancer is the leading cause of cancer-related death worldwide (1). It is the deadliest malignancy, regardless of the incidence rate (11.4%) or the fatality rate (18.0%), according to the 2020 Global Cancer Annual Report (2). Non-small cell lung carcinoma (NSCLC) accounts for 85% of all lung cancer cases (3). Numerous recurrent genetic alterations cause NSCLC, of which KRAS is a classic example. KRAS mutations are identified in 32% of patients with NSCLC (4) and are associated with a poor prognosis and a high likelihood of disease recurrence (5). KRAS is an oncogenic driver and its mutation can directly accelerate lung tumor growth. Therefore, it is considered a prospective therapeutic target and a possible diagnostic marker or biomarker for NSCLC-targeted therapy (6). Accordingly, the development of therapeutic drugs that target KRAS mutations is one of the most successful lung cancer treatments currently available. AMG-510 (Sotorasib) is a potent, orally bioavailable, and selective $KRAS^{G12C}$ covalent inhibitor with anti-tumor activity. In a single-group, phase 2 trial, treatment-related adverse events occurred in 88 of 126 patients (69.8%), including grade 3 events in 25 patients (19.8%) and a grade 4 event in 1 (0.8%) (7). In addition, the response rate of patients with NSCLC to AMG-510 is only 37% (8). It appears that the identification of effective and safe treatments for NSCLC caused by KRAS mutations remains an ongoing process.

Realgar, also known as tetra-arsenic tetra-sulfide (As_4S_4 or As_2S_2), is a traditional Chinese medicine mainly used in ancient China for deworming. However, currently it is extensively used as an anticancer treatment, particularly for malignant tumors (9) and hematological malignancies (10). The 2020

Correspondence to: Dr Dongling Liu, School of Pharmacy, Gansu University of Chinese Medicine, 35 Dingxi East Road, Lanzhou, Gansu 730000, P.R. China
E-mail: dongling83@163.com

*Contributed equally

Abbreviations: NSCLC, non-small cell lung cancer; SCL7A11, recombinant solute carrier family 7, Member 11; GPX4, glutathione peroxidase 4; ACSL4, acyl-CoA synthetase long-chain family member 4; IC_{50}, The half inhibitory concentration; ROS, reactive oxygen species; MDA, malondialdehyde; GSH, glutathione; p-, phosphorylated; Tfr1, transferrin receptor 1; TEM, transmission electron microscopy; Fer-1, ferrostatin-1; xCT, anti-glutamate-cystine antiporter

Key words: realgar, KRAS-mutant, lung cancer, apoptosis, ferroptosis, SCL7A11

edition of Chinese Pharmacopoeia stipulates that the daily dosage of realgar is between 50 mg/70 kg to 100 mg/70 kg per day. Then main content of realgar is arsenic, and the therapeutic and toxic concentrations of arsenic in human blood were 2-70 and 50-250 ng/ml, respectively. Pharmacokinetic variables were analyzed in 7 volunteers with APL and HCR by using a single dose of As_4S_4. The single dose of up to 60 mg/kg As_4S_4 was well tolerated. Arsenic could be detected in the blood 30 min after oral administration of As_4S_4. The time peak was 3.4±1.4 h and the Cmax was 24.9±8.0 μg/l (11). Clinicians demonstrated in 1995 that realgar-indigo naturalis formula-treated patients with acute promyelocytic leukemia had complete remission rates between 96.7 and 98% and a 5-year overall survival rate of 86.88% (12). Recent studies have demonstrated that realgar formulations can also be used to treat other malignancies, including NSCLC. Shi *et al* (13) demonstrated that realgar burning could improve the immunological function and hypercoagulability of patients with lung cancer. The total effective rate was 81.25%. An additional study indicated that Nano-realgar suppressed lung tumor growth *in vitro* and *in vivo* by inhibiting metabolic reprogramming (14). Moreover, in our previous study, it was shown that realgar could reduce Ras expression via the Ras/MAPK signaling pathway in *Caenorhabditis elegans* (*C. elegans*) (15), suggesting that realgar is a prospective anticancer medication that prevents Ras mutations. However, the beneficial effect of realgar in KRAS-driven lung cancer remains unknown. As a result, the emphasis of the present study was on the effects of realgar on lung cancer cells that possess KRAS mutations.

The vital KRAS-controlled pathways are important players in the growth of certain malignancies (16,17). Activation of the Ras/Raf/ERK signaling pathway is crucial for the development and spread of cancer (18). KRAS mediates mitogenic signal transduction from cell surface receptors to intracellular effectors and pathways such as Raf-MAPK (19). C-raf is the first known KRAS effector. KRAS recruits Raf proteins (A-raf, B-raf, and C-Raf) to the cell membrane, resulting in Raf activation (20,21). It has been reported that Raf inhibitors have been shown to have antitumor activity in KRAS or BRAF mutant cancers (22). Recent studies have shown that the clinical resistance to the KRAS inhibitor AMG-510 in NSCLC is characterized by various pathways, the majority of which converge on the Ras/MAPK pathway (23,24). Inhibition of Ras/MAPK is consequently a big hurdle for enhancing the efficacy in $KRAS^{G12C}$ patients (8). The process of developing KRAS inhibitors requires not only examination of the mutational status of KRAS, but also regulation of the downstream Ras signaling pathway, which can boost the effectiveness of KRAS inhibitors.

Previous studies have revealed that ferroptosis is preferentially triggered in cells overexpressing mutant Ras oncoproteins (25-27). Specific connections have been reported between ferroptosis and the KRAS mutant NSCLC. Since ferroptosis is strongly associated with cancer progression (28), patients with lung cancer have shown elevated ferritin concentrations in their serum, bronchoalveolar lavage fluid, and exhaled air condensate samples (29,30). To form erythroid cells and other cell types, transferrin receptor 1 (Tfr1) controls the intake of transferrin-bound circulating iron levels (31). In 88% of NSCLCs, Tfr1 is significantly expressed implying that lung cancer cells may be able to boost iron intake by enhancing the effects of the transferrin protein and the transferrin protein receptor. Increased Tfr1 expression is hypothesized to be a mechanism by which Ras enriches cellular iron pools, enhancing ferroptosis sensitivity (25). In addition, Ras-selective inhibitors, including NSCLC cells, can trigger non-apoptotic, iron-dependent cell death in Ras-mutant cancer cells (32-34). Cancer cells therefore store more iron than healthy cells (35), and KRAS mutant cells are more vulnerable to ferroptosis. In the present study, the data indicated that H23, a KRAS mutant cell line, was more sensitive to realgar treatment than the non-KRAS mutant cell line H1650.

Therefore, the objective of the present study was to determine whether realgar has an impact on KRAS-mutant lung cancer cells and the potential correlation between ferroptosis and the Ras/Raf pathway. The current study aimed to provide a new clinical alternative for the treatment of KRAS-mutant NSCLC tumors.

Materials and methods

Preparation of realgar solution. According to the Chinese Pharmacopoeia, realgar from Shimen (Hunan, China) was refined and identified. Briefly, 100 ml purified water and 0.1% NaOH were added to 1 g realgar powder. The solution was stirred overnight to spread evenly. The supernatant was subsequently washed with 0.1 mol/l HCl until the pH reached 7.38. The solution was filtered through a 0.22-μm microporous filter to be sterilized, sealed and refrigerated at 4˚C. By using inductively coupled plasma mass spectrometry, the concentration of total arsenic in solution was determined. Following assessment, the realgar solution had a total arsenic concentration of 2,592.067 μg/ml.

Cell culture and experimental groups. KRAS mutant H23, A549 and H460 cells, as well as non-KRAS mutant H1650 cells, were cultured in RPMI-1640 (cat. no. SH30809.01; Hyclone; Cytiva;) with 10% fetal bovine serum (cat. no. 11011-8611; Evergreen; www.hzsjq.com). The cells were incubated at 37˚C in a 5% CO_2 incubator, digested with trypsin (0.25%; Servier) and seeded into plates once they reached the logarithmic growth phase. Control, AMG-510 (10 μg/ml), realgar (1, 2 and 4 μg/ml), ferrostatin-1 (Fer-1, 1 μM), and sorafenib (8, 16 and 32 nM) were used for the experimental groups. During the logarithmic growth phase, all cells used in the experiments were harvested.

MTT assay. Cell viability was determined using the MTT assay. In 96-well plates, the cells were seeded at a density of $5x10^4$ cells/ml. The cells were subsequently treated for 24 or 48 h with a specific concentration of realgar. MTT assay was performed by adding 20 μl of MTT reagent (cat. no. M8180; Beijing Solarbio Science & Technology Co., Ltd.) into each well and continued with incubation for 4 h. After removing the supernatant, 150 μl of DMSO (cat. no. G0004; Beijing Solarbio Science & Technology Co., Ltd.) was mixed and then placed on a plate shaker to dissolve formazan crystals. A microplate reader was used to measure the absorbance at 570 nm (Bio-Rad Laboratories, Inc.). The following formula was used to calculate cell viability: Cell viability=(OD experimental

group-OD blank control group)/(OD normal group-OD blank control) x100%.

Hoechst 33258 staining assay. Nuclear morphology was examined with Hoechst 33258 staining to assess cell apoptosis. A six-well plate was used and the cells were plated at a density of $1x10^6$ cells/ml. The cells were fixed in 4% paraformaldehyde at room temperature for 15 min following 24 or 48 h of specific intervention. Subsequently, the cells were gently rinsed three times with PBS prior to incubation in the dark for 30 min at 37˚C with 1 ml (5 μg/ml) Hoechst 33258 solution in each well. The images were captured and analyzed using an Olympus IX71 fluorescence microscope (Olympus Corporation) with an excitation wavelength range of 330-380 nm.

Apoptosis measurement. Annexin V/propidium iodide (PI) double labeling was used to assess the induction of apoptosis in H23 and H1650 cells. Annexin V/PI staining was carried out according to the manufacturer's instructions using an apoptosis detection kit [cat. no. MA0220-Jun-25G; Multi Sciences (lianke) Biotech, Co., Ltd.]. Following harvesting and staining with Annexin V/PI, the treated cells were analyzed using flow cytometry (FACS CelestaTM; BD Biosciences). FlowJo was used to analyze the data (version 10.6.2; FlowJo LLC).

Transcriptomic analyses performed through RNA sequencing. Briefly, mRNA was isolated using the Isolate RNA mini kit (Bioline) and converted into cDNA. Subsequently, cDNA was sequenced in a 150 bp paired-ended fashion on the Illumina NovaSeq6000 to a depth of 40 million reads at the Amsterdam UMC Genomics Core Facility. The quality control of the reads was performed with FastQC (v0.11.2) and summarization through MultiQC (v1.0). Differential expression (DE) analysis was performed using the limma (v3.32.10) package DESeq2 (v1.28.0) in the R statistical environment (v3.46.0). Differentially expressed genes (DEGs) were defined as genes whose difference presented a limma |log2FC|>=1 and P-Value <=0.05. Functional analysis for genes in the key module was performed using Metascape (https://metascape.org/gp/index.html#/main/step1) and Gene Ontology (GO) was performed using the DAVID 6.8 database (https://david.ncifcrf.gov) to elucidate the mechanism of realgar in the treatment of H23. Subsequently, building protein-protein interaction (PPI) Network with Cytoscape (V3.8.2; http://www.cytoscape.org/).

Reactive oxygen species (ROS) detection. To detect the intracellular ROS levels in H23 cells, a ROS Assay kit (cat. no. S0033S; Beyotime Institute of Biotechnology) was used. Realgar-treated cells were incubated for 20 min with 10 μM dichlorofluorescin diacetate. Prior to counting the cells with a flow cytometer (BD Biosciences), they were washed in PBS. FlowJo was used to analyze the average fluorescence intensity (version 10.6.2; FlowJo LLC).

Measurement of Fe^{2+}, glutathione (GSH), and malondialdehyde (MDA) levels. A reduced GSH assay kit (Nanjing Jiancheng Bioengineering Institute), Ferro Orange (Dojindo Molecular Technologies, Inc.), and an MDA assay kit (Nanjing Jiancheng Bioengineering Institute) were used to measure GSH, Fe^{2+} and MDA levels, respectively.

Measurement of mitochondrial membrane potential. The membrane potential of H23 cells was determined using a mitochondrial membrane potential assay kit and JC-1 (Beijing Solarbio Science & Technology Co., Ltd.). H23 cells were seeded in a six-well plate and stained with JC-1 in the working solution for 20 min prior to flow cytometry analysis (BD Biosciences).

Transmission electron microscopy (TEM). H23 cells in the logarithmic growth phase were cultivated in six-well plates with 2 ml cell suspension per well for 48 h in culture medium containing different concentrations of realgar. The cells were digested by trypsin without EDTA, prepared following fixation in 2.5% glutaraldehyde 4 h and stored at 4˚C, and observed using TEM (Hitachi, Ltd.).

Western blotting and antibodies. The following commercially available antibodies were used: Rabbit anti-c-Raf antibody (1:1,000; cat. no. cst-9422T), rabbit anti-phosphorylated (p)-c-Raf antibody (1:1,000; cat. no. cst-9427T), rabbit anti-ERK1/2 antibody (1:1,000; cat. no. cst-4695T), rabbit anti-p-ERK1/2 antibody (1:2,000; cat. no. cst-4370T), rabbit anti-JNK antibody (1:1,000; cat. no. cst-9252T), rabbit anti-p-JNK antibody (1:1,000; cat. no. cst-4668T), rabbit anti-p38 antibody (1:1,000; cat. no. cst-8690T) and rabbit anti-p-p38 antibodies (1:1,000; cat. no. cst-4511T) were purchased from Cell Signaling Technology, Inc. A rabbit anti-glutamate-cystine antiporter (Xct/SCL7A11; 1:1,000; cat. no. ab175186) antibody was obtained from Abcam. The rabbit anti-acyl-CoA synthetase long chain family member 4 (ACSL4) antibody (1:1,000; cat. no. abs106075), rabbit anti-glutatione peroxidase (GPX) 4 antibody (1:1,000; cat. no. abs136221), anti-GAPDH (cat. no. abs830030ss) and anti-rabbit/mouse IgG, horseradish peroxidase (HRP)-linked antibody (1:10,000; cat. no. abs20040ss) were obtained from Absin (www.absin.cn).

Western blotting was used to assess the changes in protein expression. Protein extracts were isolated from each group cells using RIPA protein lysis buffer containing 1 mM PMSF (cat. no. R0010; Beijing Solarbio Science & Technology Co., Ltd.). They were centrifuged at 10,000 x g for 15 min at 4˚C. A bicinchoninic acid protein test kit was used to determine the protein concentrations (Beijing Solarbio Science & Technology Co., Ltd.). The protein lysates (30 μg) were separated by 10% SDS-PAGE and transferred to polyvinylidene fluoride membranes (EMD Millipore, 0.25 μm). The membranes were subsequently blocked in TBST buffer (TBS buffer with 0.1% Tween 20) containing 5% BSA (cat. no. PH0420; Phygene) for 2 h at room temperature. The membrane was washed three times with TBST for 10 min each prior to incubation with primary antibodies overnight at 4˚C. The membrane was subsequently incubated for 1 to 2 h at room temperature in HRP-conjugated secondary antibodies. Finally, an enhanced chemiluminescence detection kit was used with a chemiluminescence detector (C300; Azure Biosystems, Inc.) to detect HRP luminescence (Absin). Densitometric analysis was conducted to compare the expression level of proteins using ImageJ (version 1.8.0; National Institutes of Health).

Statistical analysis. The SPSS Statistics 23 software (IBM Corp.) was used for statistical analysis. GraphPad Prism (version 8.0.2; GraphPad Software, Inc.) was used for statistical

analysis of the results. One-way ANOVA was used to analyze group differences, followed by the Tukey's post-hoc test. All repeated experiments were carried out at least in triplicate. $^{*}P<0.05$ was considered to indicate a statistically significant difference.

Results

Realgar induces H23 cell apoptosis and inhibition of H23 cell proliferation. A total of 4 NSCLC cell lines (H23, A549, H460 and H1650) were applied to assess the cytotoxicity of realgar. Compared with 24, 48 h of cell treatment resulted in a larger inhibition rate which led to the selection of the 48 h time point for subsequent experiments. Following 48 h of treatment, the half inhibitory concentration (IC_{50}) values for H23, A549, and H460 were 2.66±0.33, 4.66±0.76, and 7.02±0.36 μg/ml, respectively (Table SI). This result indicated that H23 cells exhibited the higher sensitivity to realgar among the three KRAS mutant cell lines.

H1650, a non-KRAS mutant cell line, was selected as a control for the KRAS mutant cell line H23 in order to evaluate the cytotoxicity of realgar following inhibition of KRAS. When realgar was applied to both H23 and H1650 cells for 48 h, the corresponding IC_{50} values were 2.66±0.33 and 7.96±1.00 μg/ml, respectively ($P<0.01$). Following 48 h treatment of the cells with realgar, the cell morphology was assessed. It was noted that the proliferation of H23 cells was strongly inhibited by realgar, whereas the response of H1650 cells to realgar at the same concentration and time period was not as profound as that of H23 (Fig. S1). The findings revealed that realgar was highly effective in inhibiting the proliferation on KRAS mutant cells in a concentration-dependent manner following 48 h of treatment (Fig. 1A and B). Realgar was suggested to be a promising anticancer compound that targets KRAS. Subsequently, the investigation of the induction of apoptosis following treatment of the aforementioned cell lines with realgar was performed.

When the cells undergo apoptosis, the apoptotic cell nuclei can be densely stained from Hoechst 33258. In the present study, the number of dense and sparkle-stained dots (red arrows) was increased in realgar treatment compared with that of the control group. Concomitantly, the numbers of H23 and H1650 cells were reduced and the cells were irregularly arranged following treatment with realgar for 48 h (Fig. 1C and D). Annexin V and PI staining was also utilized to identify the number of apoptotic cells. Following 48 h of treatment with realgar, the apoptotic rates of H1650 cells and H23 cells were increased in a concentration-dependent manner (Fig. 1E-H). Furthermore, the apoptotic rate of H1650 cells treated with 4 μg/ml realgar was 8.2%, while that of H23 cells was 21.46% ($P<0.01$; Fig. 1I). The number of H1650 apoptotic cells following treatment with 8 μg/ml realgar was equivalent to that of H23 apoptotic cells following treatment with 4 μg/ml realgar. According to the results, realgar was more potent in KRAS mutant cells (H23) than in non-KRAS mutant cells (H1650). Therefore, KRAS mutant cells H23 were selected for further analysis. It was evident that realgar not only inhibited the proliferation of KRAS mutant cells, but also induced their apoptosis, thereby exerting a considerable anticancer effect.

Realgar-mediated anticancer effect involves induction of ferroptosis. Based on the aforementioned experiments, the data indicated that realgar exhibited an anticancer effect on KRAS mutant cells. To investigate further this effect, transcriptome analysis was performed on realgar-treated (2 μg/ml) H23 cells. The analysis aimed to identify potential genes regulated by realgar in order to gain insight into the molecular mechanism by which realgar inhibits lung cancer progression.

In H23 cells, realgar resulted in a >2-fold upregulation of 195 genes and >2-fold downregulation of 286 genes (Fig. 2A). Among them, the top-ranked genes HMOX1, SESN2, CYR61, and TRIB3, the remaining upregulated differentially expressed genes (DEGs), TNFRSF19, SPOCK2, CTDSP1, TRIB3, as well as other downregulated DEGs were involved in a variety of biological pathways important for cancer development. To further clarify the DEGs, a hierarchical cluster analysis was performed (Fig. 2B). The results revealed a clear color contrast between the groups examined; the color of the same cluster within a group was similar. As a result, the results of the hierarchical cluster analysis were trustworthy. Furthermore, the DAVID online platform was used to identify gene ontology enrichments, such as those for biological process, cellular component, and molecular function components. The column diagram (Fig. 2C) depicts all of their top 10 pathways (count ≥3) that are primarily related to cellular response to chemical stimulus, extracellular matrix regulation, and sulfur compound binding. The functional analysis for genes in the key module was performed using Metascape and revealed four pathways closely related to ferroptosis among the upregulated pathways, namely the p53 signaling pathway, cysteine and methionine metabolism (36), glutathione metabolism and ferroptosis. GPX4 has been shown to be a central regulator of ferroptosis and a key factor in the regulation of glutathione metabolic pathways. Among the downregulated pathways, four have been identified that are closely related to cancer as follows: The MAPK signaling pathway, the Wnt signaling pathway, the TGF-β signaling pathway, and cancer transcriptional misregulation (Fig. 2D). Using Cytoscape (degree >3), a protein-protein interaction (PPI) network with 99 nodes and 366 edges was generated, with upregulated and downregulated genes labeled in blue and red, respectively (Fig. 2E). These results revealed that the regulation of cell proliferation by realgar was closely related with the ferroptosis pathway and the MAPK signaling pathway in KRAS mutant cells.

FerrDb (http://www.zhounan.org/ferrdb/current/) is the first worldwide database that contains information on ferroptosis regulators and markers with 254 ferroptosis-related targets and ferroptosis-related illness connections. In the present study, it was found that 14 co-differentially expressed genes were identified following treatment of realgar to H23 cells and induction of ferroptosis (Fig. 2F), including HMOX1, SLC7A11, SESN2, TRIB3, OLFM4, GOT1, and SLC1A4 (Table I). A PPI network was constructed using STRING database (37) (Fig. 2G). Based on the aforementioned results, it was hypothesized that ferroptosis was the main mechanism of anticancer action of realgar. However, this hypothesis requires further validation.

Ferroptosis mediates realgar-induced H23 cell death. Transcriptome analysis indicated that realgar exerted a significant effect on KRAS mutant lung cancer cells via the

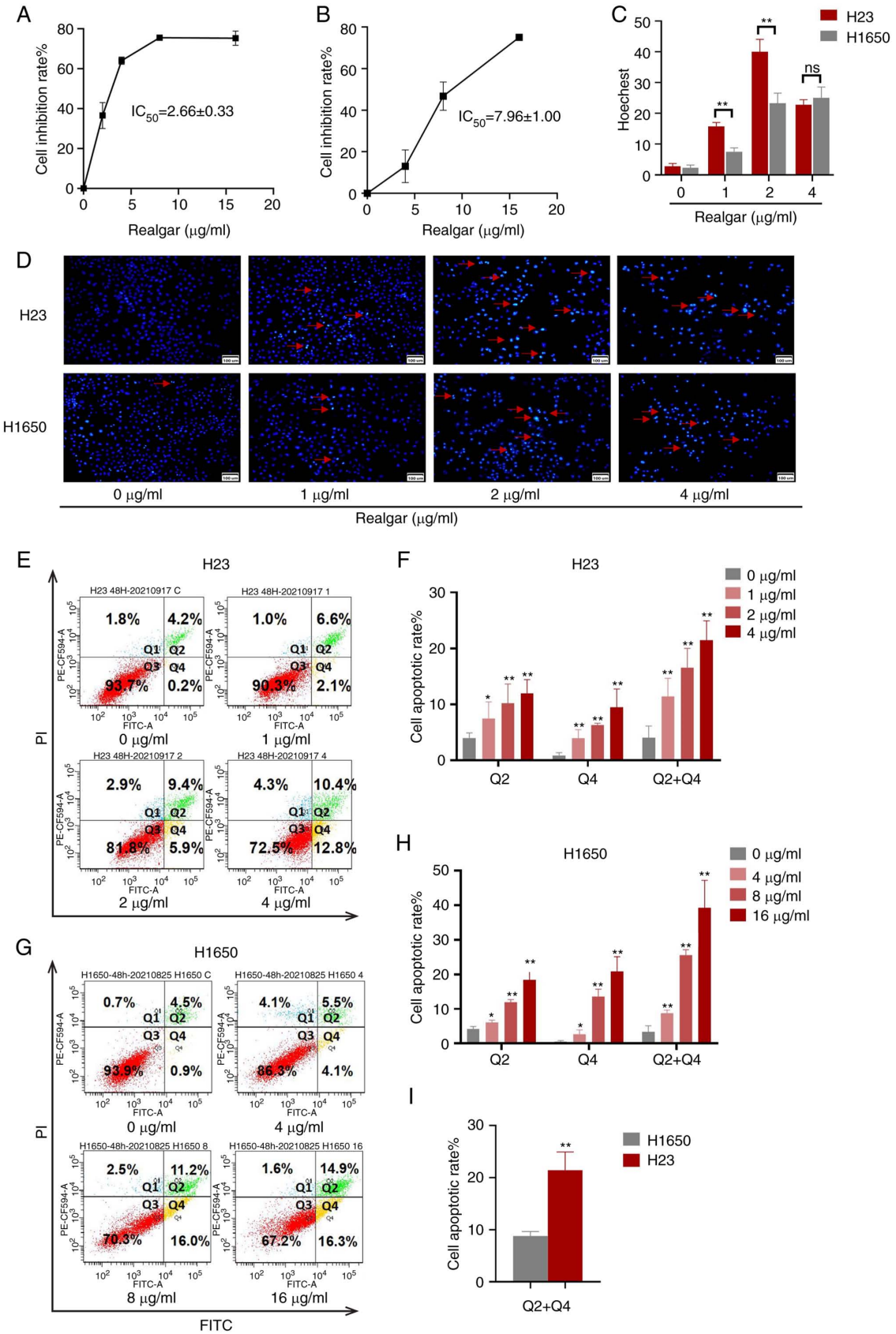

Figure 1. The cytotoxicity of realgar against H23 and H1650 cells. (A) The effects of realgar on the inhibition of H23 cells proliferation were determined at 48 h following realgar treatment. (B) The effects of realgar on the inhibition of H1650 cells proliferation were determined at 48 h following realgar treatment. (C) The quantification of apoptosis in Hoechst 33258 staining was used for H23 and H1650 cells. (D) Hoechst 33258 staining was used for H23 and H1650 cells apoptosis analysis. The apoptotic cells are highlighted by red arrows (x100). (E) H23 cells were stained with AV/PI following treatment with different concentrations of realgar for 48 h. (F) The number of H23 apoptotic cells was counted and compared with that of the control group. (G) H1650 cells were stained with AV/PI following treatment with different concentrations of realgar for 48 h. (H) The number of H1650 apoptotic cells was counted and compared with that of the control group. (I) The apoptotic rate of H1650 and H23 cells treated with 4 μg/ml realgar. All data are presented as the mean ± SD of three independent experiments. *P<0.05 and **P<0.01. AV/PI, Annexin V/propidium iodide; ns, not significant.

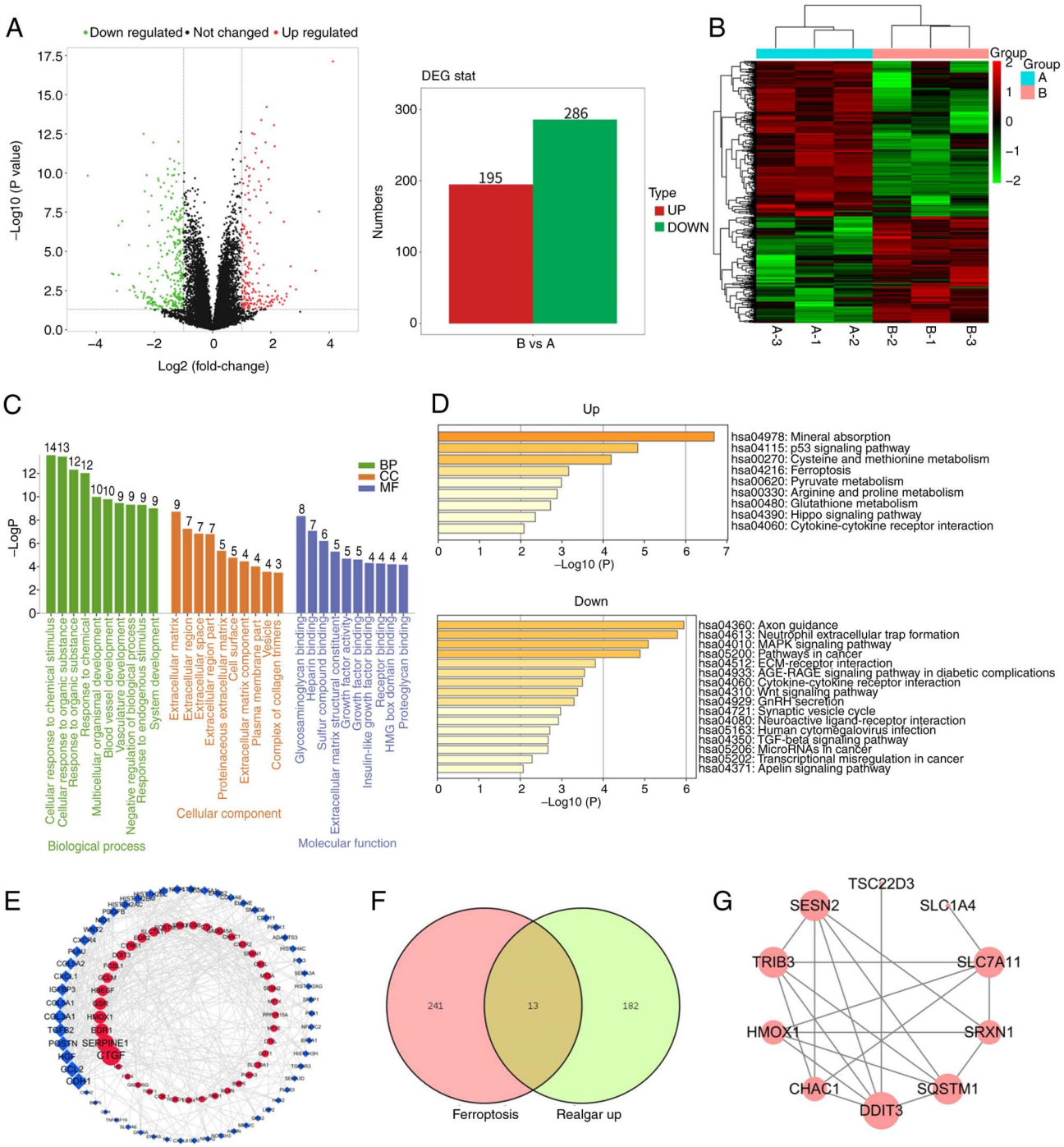

Figure 2. Transcriptome analysis of realgar-treated H23 cells. (a) H23 cells without realgar treatment; (b) H23 cells with realgar treatment (2 μg/ml). (A) Determination of DEGs by volcano plots. (B) Heatmap analysis and the relative contents (red and green areas represent high and low expression, respectively). (C) GO enrichment analysis of DEGs. (D) KEGG pathway enrichment analysis of the upregulated and downregulated genes. (E) PPI network analysis of the upregulated and downregulated genes. (F and G) Venn and PPI diagrams of realgar-related gene and ferroptosis-related gene intersection. DEGs, differentially expressed genes, GO, gene ontology; KEGG, Kyoto Encyclopedia of Genes and Genomes; PPI, protein-protein interaction.

induction of ferroptosis. Therefore, subsequent analysis was performed to assess whether ferroptosis was actually involved in the mechanism of action of realgar.

In order to examine the function of ferroptosis in the inhibition of H23 cell proliferation caused by realgar, several studies were previously carried out. The intracellular iron ions are accumulated during ferroptosis (38). Excessive free iron boosts the Fenton reaction, which produces ROS when the iron balance is disrupted. This will in turn facilitate lipid peroxidation and cause cell death (39). MDA is a marker of lipid peroxidation and GSH is an intracellular antioxidant; both play significant roles in the induction of cell ferroptosis (40). The current results indicated that Fe^{2+}, GSH, MDA and ROS levels were altered in a dose-dependent manner following treatment with realgar. Treatment of the cells with realgar caused a 1.86-fold increase in the intracellular Fe^{2+} (Fig. 3A) than the corresponding levels noted in the control cells ($P<0.01$). ROS levels were increased 0.71-fold compared

Table I. The intersection genes identified following comparison of the DEGs of realgar-associated treatment and those of considered as ferroptosis targets.

Symbol	Features in ferroptosis
SLC7A11	Suppressor, Marker
HMOX1	Driver, Suppressor, Marker
SESN2	Suppressor, Marker
TRIB3	Marker
GOT1	Driver
SLC1A4	Marker
SQSTM1	Suppressor
PCK2	Marker
CHAC1	Driver, Marker
TSC22D3	Marker
DDIT3	Marker
SLC2A8	Marker
SRXN1	Marker
AIFM2	Suppressor

Driver-Genes that promote the induction of ferroptosis; suppressor-genes that prevent the induction of ferroptosis; marker-genes that indicate the occurrence of ferroptosis. DEGs, differentially expressed genes.

with those noted in the control cells (Fig. 3B). GSH levels were decreased following realgar treatment (Fig. 3C), while the MDA levels (Fig. 3D) were elevated. Therefore, realgar could indeed cause induction of ferroptosis of KRAS mutant cells.

Iron is metabolized primarily by the mitochondria through the iron catabolic, anabolic, and utilization pathways, all of which are connected to the ferroptosis process (41). The mitochondrial apoptosis process depends on the mitochondrial membrane potential (MMP). MMP may be downregulated concurrently with ferroptosis causing an alteration in the mitochondrial membrane structure (42). Therefore, the mitochondrial morphology and MMP serve as indicators of ferroptosis. TEM is the gold standard for detecting mitochondrial abnormalities; therefore, JC-1 labeling was employed to assess mitochondrial damage in H23 cells. The ultramorphological features showed that the cell membrane was broken and blistered, the mitochondria became smaller, the membrane density increased, the mitochondrial ridge decreased or disappeared, the outer membrane of mitochondria was broken, the size of nucleus was normal, but lack of chromatin condensation. Specifically, mitochondria appeared smaller and the inner membrane folding was disturbed (Fig. 3E). However, as the concentration increases the cell membrane ruptures, thus it was hypothesized that ferroptosis occurred under the action of 2 μg/ml of realgar. Following treatment of H23 cells with realgar, the aggregated JC-1 levels in the mitochondria were decreased, whereas the monomeric JC-1 levels were increased (Fig. 3F). The data implied that realgar had the potential to alter the mitochondrial energy metabolism, which was essential for the induction of ferroptosis.

Western blotting (Fig. 3G) was used to compare the expression levels of specific proteins in the control and realgar groups. The ferroptosis negative regulatory proteins that have been identified to date are GPX4 and cysteine/glutamate transporter (SLC7A11/xCT). GPX4 eliminates lipid peroxides by employing GSH as a reducing agent and lipid ROS as the main substrate (43). SLC7A11/xCT facilitates the transfer of cystine, a GSH precursor, and is a key negative regulatory protein of ferroptosis (44). ACSL4 is a crucial ferroptosis positive regulatory protein that can facilitate the increase in lipid ROS levels and induce ferroptosis (45). The results of the present study indicated that GPX4 (0.65-fold, $P<0.01$) and SCL7A11 (0.75-fold, $P<0.05$) levels were significantly lower in cells treated with 4 μg/ml realgar than those noted in the control group, while ASCL4 levels were increased dose-dependently (2.70-fold, $P<0.01$; Fig. 3H) which were consistent with the RNA sequencing results.

These findings demonstrated that realgar increased the key monitor of ferroptosis in KRAS mutant H23 cell lines. To verify this hypothesis, Fer-1 was added, a ferroptosis inhibitor, and results showed that Fer-1 abolished the increase in cell death caused by realgar (Fig. 3I). The levels of Fe^{2+}, GSH and MDA were also reversed by Fer-1 by 29.17, 13.82, 16.62%, respectively in 2 μg/ml realgar (Fig. 3J-L).

Ras/MAPK pathway plays a critical role in realgar's anticancer activity of KRAS mutant cells. The initiation and development of ferroptosis is influenced by a variety of signaling pathways and variables, although it is predominantly caused by the metabolism of amino acids and iron, the lipid peroxidation, and the levels of lipid ROS (46). The ferroptosis pathway is activated by redundant glutamate, which also phosphorylates certain MAPKs, such as ERK, JNK, and p38 (47). Based on a previous study, it was discovered that realgar could downregulate Ras expression via the Ras/MAPK signaling pathway in a *C. elegans* model (15). To further investigate the mechanism of realgar in H23 cells, western blotting was used to examine the expression levels of the related signaling proteins following 48 h of cell exposure to realgar. JNK and p38 levels were not significantly altered, whereas p-JNK and p-p38 protein levels were significantly increased (2.74- and 1.71-fold, respectively) following treatment of H23 cells with realgar for 48 h (Fig. 4A). Realgar inhibited p-ERK1/2 and p-Raf protein levels in H23 cells following 48 h of treatment (Fig. 4B), whereas the levels of ERK1/2 and Raf were not affected. These findings suggested that the anticancer activity of realgar may be associated with the Ras/MAPK pathway.

Realgar induces ferroptosis in KRAS-mutated H23 cells by targeting Raf. The Ras/Raf/MEK/ERK pathway is crucial in oncogenesis and cancer progression (18). Because all Raf family members act directly downstream of Ras, they are also important factors in oncogenesis, mediating the effects of mutated Ras (48). To further study the functional involvement of ferroptosis in the realgar-activated Ras/Raf/JNK/ERK pathway in KRAS-mutant NSCLC, H23 cells were exposed to Fer-1 for 4 h. The result showed that Fer-1 could abolish realgar-induced cell death (Fig. 3I) and restore p-Raf protein levels in realgar-treated H23 cells (Fig. 4D), while realgar enhanced p-p38 and p-JNK protein levels but had no effect on Fer-1 (Fig. 4C and D). It was hypothesized that realgar-induced ferroptosis was primarily related to Raf and not JNK/ERK.

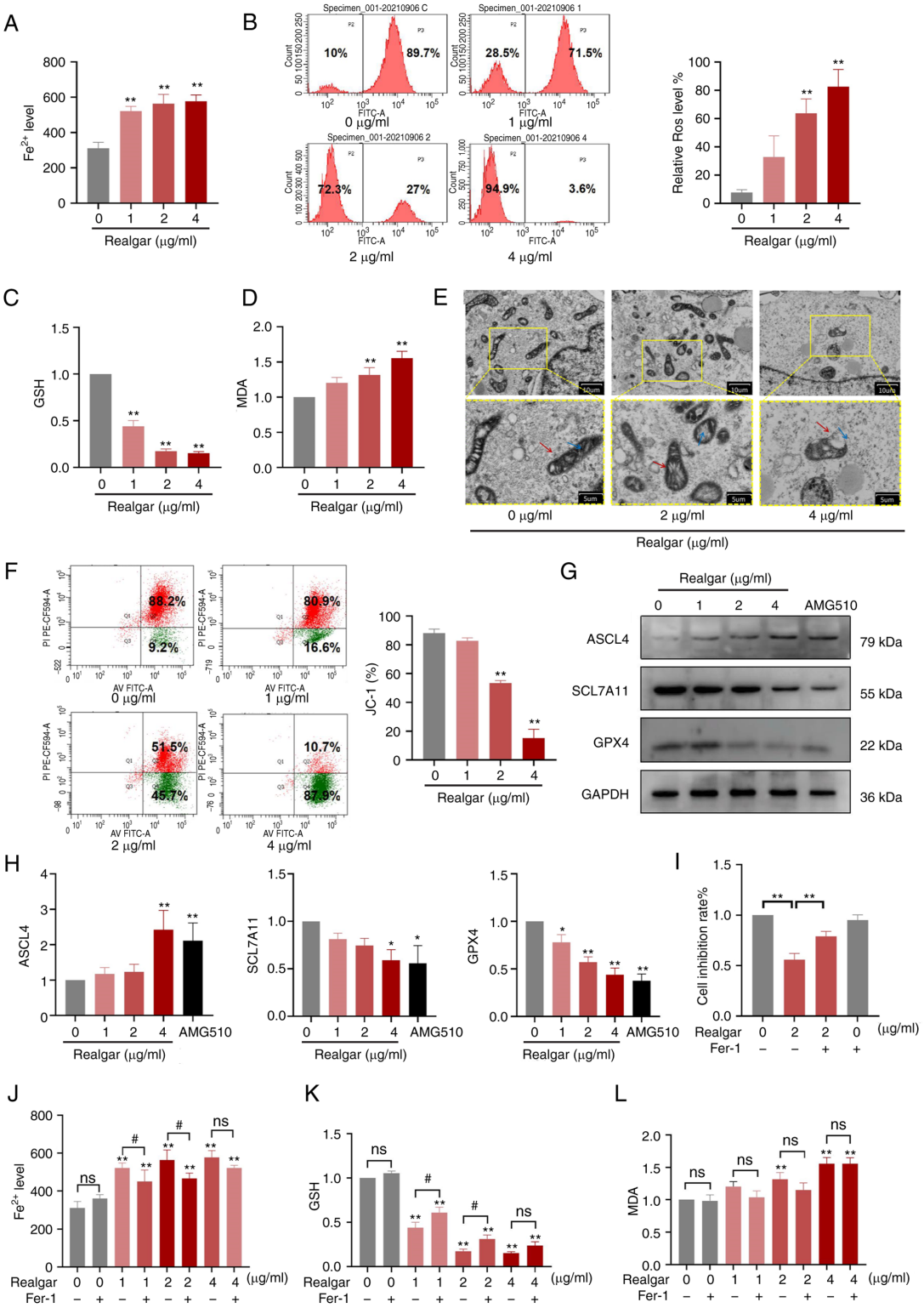

Figure 3. Realgar induces ferroptosis, which is linked to cell death. (A) The intracellular Fe2+ levels in H23 cells were measured. (B) ROS levels in H23 cells following treatment with different concentrations of realgar. (C) GSH reduction in H23 cells treated with realgar. (D) Increase in MDA levels of H23 cells treated with realgar. (E) Morphological changes in mitochondria isolated from H23 cells following 48 h of realgar treatment at 2 μg/ml or 4 μg/ml. Two images are presented for each group and the scale is marked on the bottom right of each image. The diagram is an expanded version of the yellow box area. The red arrow represents the mitochondrial membrane, while the blue arrow represents the cristae. (F) Flow cytometry was used to measure the intracellular JC-1 levels. (G) Western blot analysis of ferroptosis markers. (H) Indicating a decrease in the expression levels of GPX4 and SCL7A11 and an increase in the expression levels of ASCL4 in H23 cells following realgar treatment. (I) H23 cells were incubated with 2 μg/ml realgar for 48 h and subsequently pre-treated with Fer-1 for 4 h. (J) The intracellular iron levels were determined in H23 cells by using a Fe^{2+} iron probe known as Ferro Orange. Realgar increased the concentration levels of Fe^{2+}; this effect was reversed by the ferroptosis rescue agent Fer-1 (1 μM). (K) The reduction of GSH in H23 cells treated with realgar was reversed by the ferroptosis rescue agent Fer-1 (1 μM). (L) The increase in the concentration levels of MDA was detected in H23 cells following treatment with realgar. All data are presented as the mean ± SD of three independent experiments. *P<0.05 and **P<0.01 compared with the control group. $^{\#}$P<0.05 compared with realgar treatment at different concentrations. AMG-510=10 μg/ml. GPX4, glutathione peroxidase 4; SCL7A11, recombinant solute carrier family 7, member 11; ASCL4, acyl-CoA synthetase long-chain family member 4; ROS, reactive oxygen species; GSH, glutathione; MDA, malondialdehyde; Fer-1, ferrostatin-1; ns, not significant.

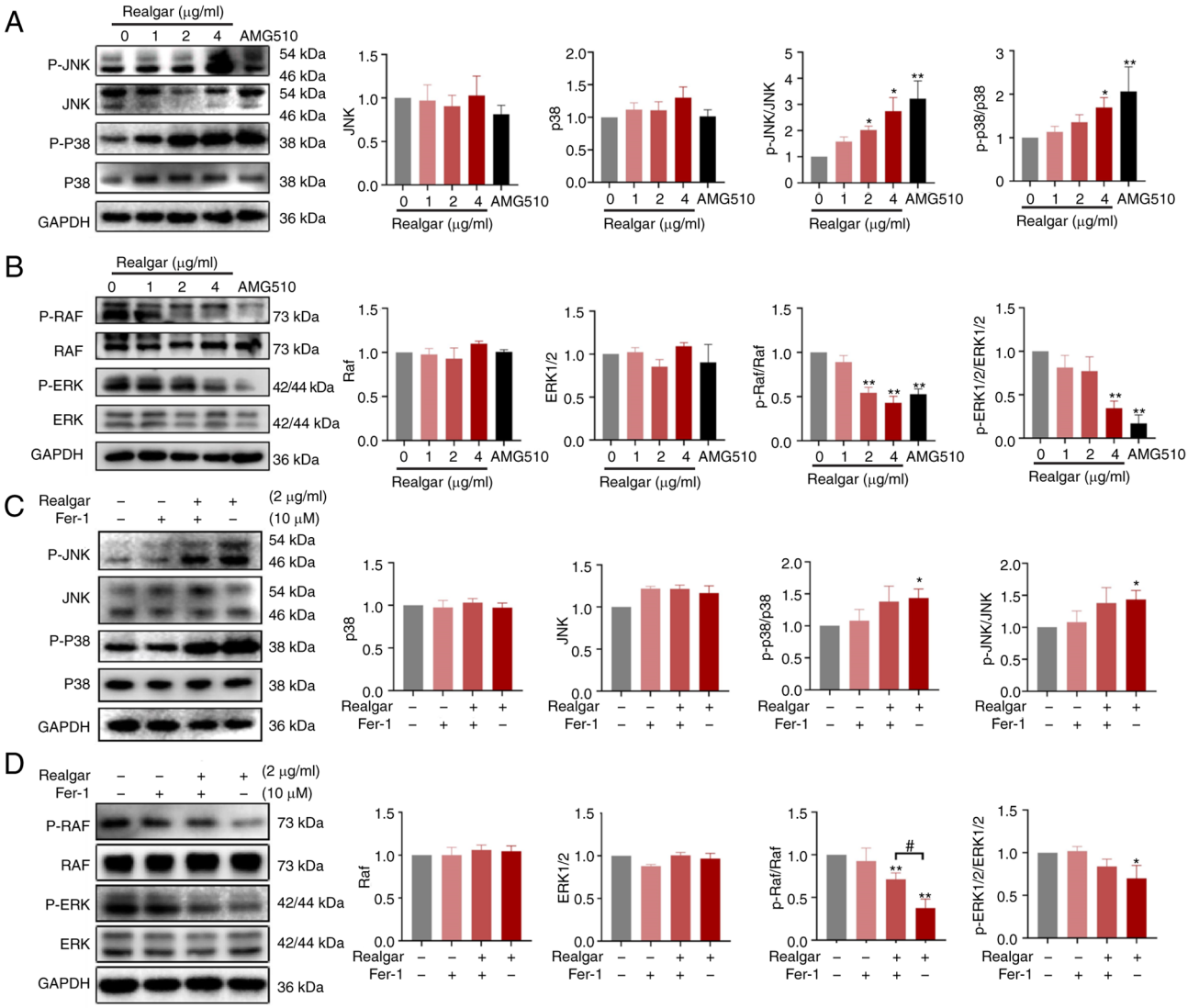

Figure 4. The effects of realgar on the phosphorylation of Raf, ERK1/2, JNK, and p38. (A) The protein expression levels of JNK and p38 MAPK were detected by western blotting following treatment of the cells with different concentrations of realgar for 48 h. (B) The protein expression levels of Raf and ERK1/2 were detected by western blotting following treatment of the cells with different concentrations of realgar for 48 h. (C) The protein expression levels of JNK and p38 MAPK were detected by western blotting following treatment of the cells with different concentrations of realgar for 48 h and then pre-treated with Fer-1 for 4 h. (D) The protein expression levels of Raf and ERK1/2 were detected by western blotting following treatment of the cells with different concentrations of realgar for 48 h and then pre-treated with Fer-1 for 4 h. All data are presented as the mean ± SD (n=3). *P<0.05 and **P<0.01 compared with the control group. $^{\#}$P<0.05 compared with realgar treatment group. AMG-510=10 μg/ml. p-, phosphorylated.

Then, Sorafenib was added, a Raf inhibitor, to examine the role of Raf in realgar-induced ferroptosis. Using the MTT assay, the effects of Sorafenib on the growth of H23 cells were analyzed (Fig. 5A). H23 cells were treated either with 16 nM sorafenib or 2 μg/ml realgar alone or in combination for 48 h. Cell viability was decreased by an average of 61.09±0.07 and 57.10±0.05% in Sorafenib and realgar, respectively. However, after the addition of Sorafenib, realgar reduced cell viability more effectively to 39.40±0.05% (Fig. 5B). Simultaneously, Sorafenib also altered the expression of ferroptosis-related proteins SCL7A11, GPX4 and ASCL4. These results (Fig. 5C and D) showed that after treatment with Sorafenib, realgar significantly decreased the expression of SCL7A11 and GPX4 proteins while increasing the expression of ASCL4 in H23 cells compared with cells treated with realgar alone.

Consequently, realgar-induced ferroptosis may be targeted to regulate Raf kinase, thereby further regulating the downstream JNK/ERK signaling cascade to suppress KRAS cells and exert an anticancer activity.

Discussion

KRAS mutant lung cancer remains to find effective therapeutic treatment. Realgar has demonstrated an optimal anticancer effect (49,50). One of the main goals of the present study was to assess the effect of this compound on lung cancer cells with KRAS mutations. According to our findings presented, realgar exhibited selectivity for the KRAS mutant H23 cells compared with non-KRAS mutant H1650 cells. The inhibition ratio followed a dose-dependent manner in both of these cell lines and realgar induced apoptosis more efficiently

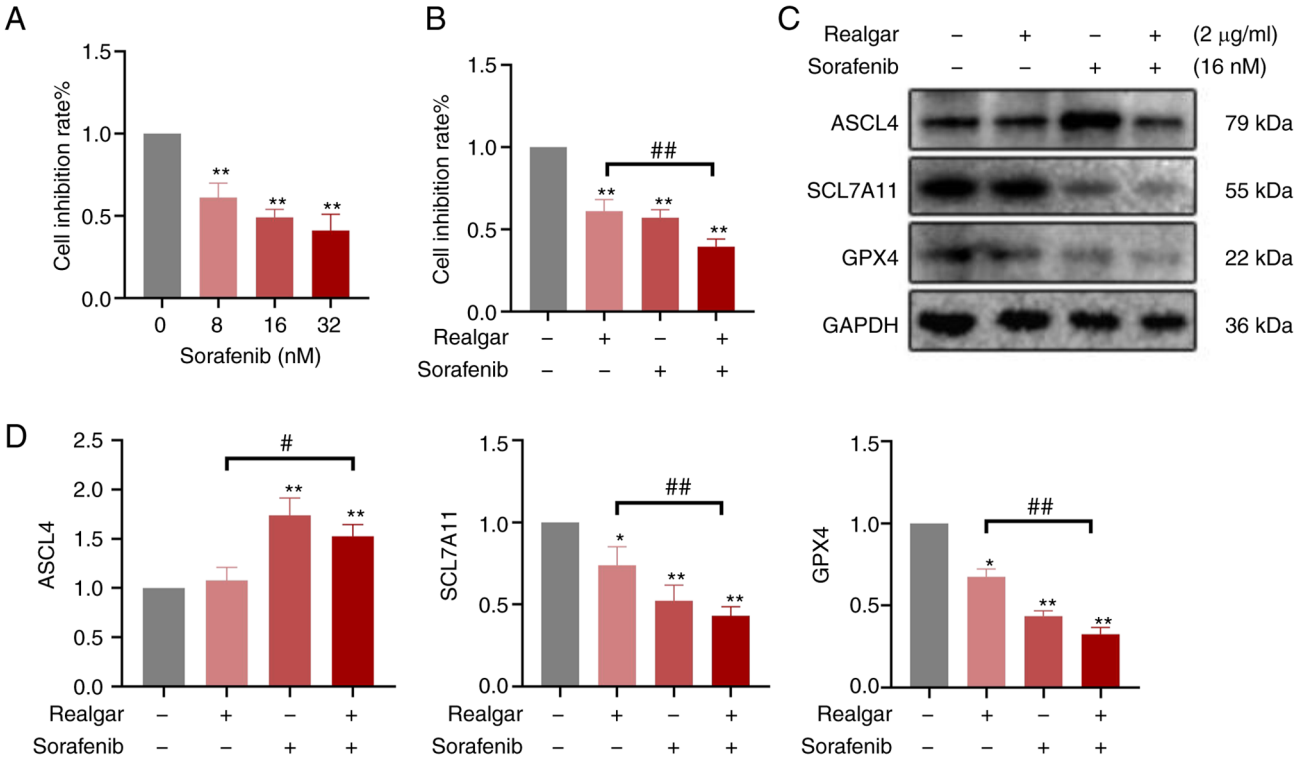

Figure 5. (A) Cell viability of H23 cells with different concentrations of sorafenib for 48 h was detected by MTT. (B) H23 cells with or without of sorafenib (16 nM) and realgar (2 μg/ml), and cell viability was assayed by MTT. (C and D) H23 cells with or without of sorafenib (16 nM) and realgar (2 μg/ml), and western blot analyses of SLC7A11, GPX4 and ASCL4 proteins were performed. *P<0.05 and **P<0.01 compared with the control group. $^{\#}$P<0.05 and $^{\#\#}$P<0.05 compared with realgar treatment group.

in H23 cells. JNK and p38 have been shown to regulate a number of transcription factors, increasing the production of pro-apoptotic proteins while decreasing the expression of anti-apoptotic proteins (8). Through both transcriptional and post-translational mechanisms, ERK can be anti-apoptotic by upregulating anti-apoptotic proteins and downregulating pro-apoptotic proteins (51). On controlling cell survival and apoptosis, they have been shown to have opposite effects. According to Huang *et al* (52), arsenic trioxide (ATO)-induced p38 MAPK overexpression promotes apoptosis in K562 and MEG-01 cells. According to Wu *et al* (53), activated p38 MAPK is a pro-apoptotic signal for curcumin-induced mortality of chemoresistant human lung cancer cells A549. Theabrownin, a component of green tea, suppresses human NSCLC in a xenograft model via activating the MAPK/JNK signaling pathway, according to Xiao *et al* (54). Liu *et al* (55) found that elevated KLHL17 in NSCLC promotes tumor growth and migration via activating the Ras/MAPK signaling pathway. The MEK inhibitor, on the other hand, enhances growth inhibition and cell death in Calu-6 lung cancer cells treated with ATO (56). JNK and p38 will be activated while ERK is suppressed in order to cause apoptosis in cancer cells, as evidenced by the effects of dominant-interfering or constitutively active versions of particular JNK-p38 and ERK signaling pathway components (57). Lee *et al* (58) reported that As_4S_4 could decrease the expression levels of specific proteins, such as Bcl-2 and p-ERK in the KRAS mutant cell lines A549 and H460 and exert an antiangiogenic effect, which led to the inhibition of tumor cell growth, proliferation, invasion, and metastasis. However, since tumor cells exhibit antiapoptotic properties, novel molecular techniques were used in the current study to assess their multiple mechanisms of action.

It is known that ferroptosis levels in tumor tissues are typically higher than those noted in adjacent normal tissues. Moreover, these levels are related to drug sensitivity, cancer metastasis, clinical characteristics, and clinical outcomes (59). Transcriptomic sequencing analysis has been widely used to identify novel pathways so as to improve the diagnosis and therapy of a number of disorders, including cancer, immune system diseases, and infectious diseases (60). Research revealed that realgar may exert an anticancer effect by modulation of the p53 signaling pathway (61), cysteine, methionine, and glutathione metabolic pathways. It is interesting to note that all of these pathways are considered to be active during ferroptosis. Our results also showed that ferroptosis pathway was involved in the impact of realgar on KRAS mutant H23 cells. Therefore, it was proposed that ferroptosis plays an important role in the effect of realgar on cancer cells.

Recent studies have revealed that ferroptosis is essential for the development of malignancies, particularly lung cancer (26), and is considered to be a potential therapeutic target for Ras-mutant malignancies as the Ras mutation has been shown to enhance the iron excess in cells and make them more vulnerable to substances that promote ferroptosis (32). The activation of xCT transcription enables oncogene KRAS to shield cells from oxidative stress by increasing intracellular GSH levels (62). This therapy-resistant tumor may respond to xCT preserving redox balance and aiding oncogenic KRAS-mediated transformation (63). As a crucial structural element of the Xc cell system and a potential biological marker, SLC7A11 has been to shown to

be highly expressed in NSCLC (64). The inhibition of SLC7A11 mediates KRAS mutant lung cancer cell death by decreasing lung cancer cell growth and metastasis *in vitro* and *in vivo* (65). According to Zhang *et al* (66), upregulation of SLC7A11 expression reduces ferroptosis in A549 and H1299 cells, promoting the growth and spread of the tumors. Liu *et al* (67), found that capsaicin reduces the growth of the KRAS mutant lung cancer cell lines A549 and NCI-H23 and induces ferroptosis by silencing SLC7A11/GPX4 signaling. Zhao *et al* indicated that Fuzheng Kang'ai decoction induced ferroptosis in NSCLC by inhibiting GPX4. Our data also showed the expression levels of the ferroptosis-promoting signaling pathway protein ACSL4 were substantially increased in the presence of 4 μg/ml realgar, whereas the expression levels of the ferroptosis-inhibiting signaling pathway proteins GPX4 and xCT were notably downregulated. Thus, regulating the SLC7A11/GPX4 pathway and increasing the protein level of ACSL4 is one of the crucial mechanisms for realgar-mediated ferroptosis to play an anticancer role. In addition, realgar may result in a large decrease in intracellular GSH and an increase in MDA content and intracellular ROS levels as well as cell mitochondrial shrinkage. As revealed in the present study, the number of mitochondrial ridges was dramatically reduced compared with that of the control group. These findings confirmed once again that realgar-induced ferroptosis was the cell death-mediated mechanism of KRAS mutant H23 cells. The improvement of the expression levels of the aforementioned ferroptosis-related markers (Fe^{2+}, GSH and MDA) by Fer-1 suggests that further confirming that ferroptosis occurs in KRAS mutant H23 cells exposed to realgar.

In a number of diseases, ferroptosis is intimately correlated with MAPK signaling (68). Ferroptosis may be selectively produced in cells overexpressing mutant Ras oncoproteins. The recovery effect of p-Raf was the most obvious when the ferroptosis inhibitor Fer-1 was used to interfere with the changes in the MAPK signaling pathway of H23 cells caused by realgar. According to Ma *et al* (69), lidocaine prevented ferroptosis and barrier failure in hypoxia-reoxygenation-induced A549 cells by inhibiting the p38 MAPK signaling pathway. In addition, Yang *et al* (70) demonstrated that in KRAS mutant colorectal cancer cells, cetuximab increased Ras-selective lethal (RSL3)-induced ferroptosis via the activation of p38 MAPK. L-F001 can prevent RSL3-induced ferroptosis by preserving iron homeostasis and suppressing JNK in HT22 cells (71). This demonstrated the powerful MAPK-mediated crosstalk mechanism between apoptosis and ferroptosis (72). Meanwhile, the realgar-induced ferroptosis was also aggravated by adding to Raf inhibitor Sorafenib. However, while Sorafenib has tumor-suppressing efficacy as a single agent, its clinical application is limited by numerous complex drug resistance mechanisms and side effects. Our findings indicated that the concomitant administration of realgar and Sorafenib enhanced ferroptosis in H23 cells, suggesting that realgar may be used as a synergistic drug for Sorafenib.

The current study contains significant limitations. Not only protein expression, but also protein knockdown or knock-out model should be applied to show the unique role of realgar. The present study examined only the regulation of ferroptosis by realgar in KRAS mutant NSCLC cells, and our experimental methods can only prove that Raf plays a partial, not a full, role in realgar-induced ferroptosis. Thus, it is anticipated that different cell death pathways may be implicated in the mechanism of anticancer action of realgar. In future studies, the causal connection between ferroptosis and apoptosis and their potential to occur concurrently following treatment of lung cancer cells with realgar will be investigated. In addition, *in vivo* tests will also be performed in the future to support these findings.

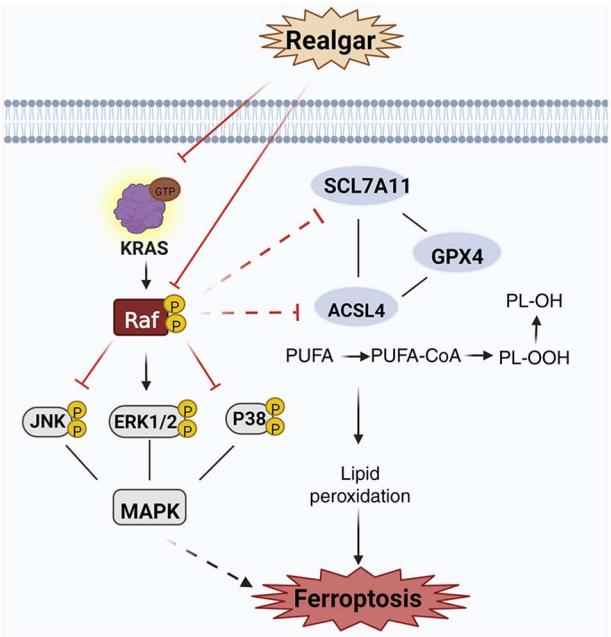

Figure 6. Realgar-induced ferroptosis may be mediated via KRAS/Raf/MAPK. Realgar may be targeted to regulate Raf kinase, thereby further regulating the downstream JNK/ERK signaling cascade to suppress KRAS cells and exert an anticancer activity. At the same time, realgar inactivating GPX4, the ability of realgar to impair Xc- or suppress GSH synthesis can result in a buildup in the lipid peroxide levels and in an increase in ferroptotic cell death by targeting Raf-mediated Ras/MAPK pathway. Two enzymes, notably ACSL4, which are required for lipid remodeling, can convert PUFAs into PUFA-PEs. Created in BioRender.com. GPX4, glutathione peroxidase 4; ROS, reactive oxygen species; GSH, glutathione; PUFA, polyunsaturated fatty acid; PE, phosphatidylethanolamine.

The findings of the present study included confirmation of the role of realgar in inducing ferroptosis in KRAS mutant NSCLC tumors and a preliminary investigation of the putative mechanisms regulating ferroptosis via the Ras/MAPK pathway (Fig. 6). In conclusion, the present study demonstrated that realgar could prevent the proliferation of lung cancer cells with a KRAS mutation and exert an anticancer function by regulating ferroptosis via targeting Raf-mediated Ras/MAPK pathway. These data provided a novel medication for NSCLC, moreover, realgar could be a co-treatment with Sorafenib for clinical therapeutic strategy.

Acknowledgements

Not applicable.

Funding

The present study was supported by the National Natural Science Foundation of China (grant nos. 81760789 and 82074419) and Research Center of Traditional Chinese Medicine, Gansu Province (grant no. zyzx-2020-21).

Availability of data and materials

All data generated or analyzed during this study are included in this published article and its Supporting Information files. The transcriptomic sequencing datasets have been submitted to a public database (NCBI). This is the associated accession numbers and password: geoftp; rebUzyi1. (ftp-private.ncbi.nlm.nih.gov).

Authors' contributions

Among the authors listed, XL and YH did the majority of the work in this study, writing the manuscript and conceptualization. JD assisted with the western blot analysis and methodology. LX revised the statistical findings and performed visualization. WH and JS assisted with the cell experiments and edited. WR concentrated primarily on the preliminary investigation and cell screening. DL designed the study, oversaw the work, and provided the study's facilities. XL and YH confirm the authenticity of all the raw data. All authors read and approved the final version of the manuscript.

Ethics approval and consent to participate

Not applicable.

Patient consent for publication

Not applicable.

Competing interests

The authors declare that they have no competing interests.

References

1. Huang J, Deng Y, Tin MS, Lok V, Ngai CH, Zhang L, Lucero-Prisno DE III, Xu W, Zheng ZJ, Elcarte E, *et al*: Distribution, risk factors, and temporal trends for lung cancer incidence and mortality: A global analysis. Chest 161: 1101-1111, 2022.
2. Sung H, Ferlay J, Siegel RL, Laversanne M, Soerjomataram I, Jemal A and Bray F: Global cancer statistics 2020: GLOBOCAN estimates of incidence and mortality worldwide for 36 cancers in 185 countries. CA Cancer J Clin 71: 209-249, 2021.
3. Herbst RS, Morgensztern D and Boshoff C: The biology and management of non-small cell lung cancer. Nature 553: 446-454, 2018.
4. Ryan MB and Corcoran RB: Therapeutic strategies to target RAS-mutant cancers. Nat Rev Clin Oncol 15: 709-720, 2018.
5. Nagasaka M, Li Y, Sukari A, Ou SI, Al-Hallak MN and Azmi AS: KRAS G12C game of thrones, which direct KRAS inhibitor will claim the iron throne? Cancer Treat Rev 84: 101974, 2020.
6. Rodak O, Peris-Díaz MD, Olbromski M, Podhorska-Okołów M and Dzięgiel P: Current landscape of non-small cell lung cancer: Epidemiology, histological classification, targeted therapies, and immunotherapy. Cancers (Basel) 13: 4705, 2021.
7. Skoulidis F, Li BT, Dy GK, Price TJ, Falchook GS, Wolf J, Italiano A, Schuler M, Borghaei H, Barlesi F, *et al*: Sotorasib for lung cancers with KRAS p.G12C mutation. N Engl J Med 384: 2371-2381, 2021.
8. Ryan MB, Coker O, Sorokin A, Fella K, Barnes H, Wong E, Kanikarla P, Gao F, Zhang Y, Zhou L, *et al*: KRAS^{G12C}-independent feedback activation of wild-type RAS constrains KRAS^{G12C} inhibitor efficacy. Cell Rep 39: 110993, 2022.
9. Xiaoxia X, Jing S, Dongbin X, Yonggang T, Jingke Z, Yanying Z and Hulai W: Realgar nanoparticles inhibit migration, invasion and metastasis in a mouse model of breast cancer by suppressing matrix metalloproteinases and angiogenesis. Curr Drug Deliv 17: 148-158, 2020.
10. Wang L, Zhou GB, Liu P, Song JH, Liang Y, Yan XJ, Xu F, Wang BS, Mao JH, Shen ZX, *et al*: Dissection of mechanisms of Chinese medicinal formula realgar-indigo naturalis as an effective treatment for promyelocytic leukemia. Proc Natl Acad Sci USA 105: 4826-4831, 2008.
11. Lu DP, Qiu JY, Jiang B, Wang Q, Liu KY, Liu YR and Chen SS: Tetra-arsenic tetra-sulfide for the treatment of acute promyelocytic leukemia: A pilot report. Blood 99: 3136-3143, 2002.
12. Huang SL, Guo AX, Xiang Y, Wand XB, Lin HX and Fu L: Clinical study on the treatment of acute promyelocytic leukemia with composite indigo naturalis tablets. Chin J Hematol 16: 26-28, 1995.
13. Shi G and Shan G: Effects of yellow loquat on changes in immune function, hemorheology and coagulation function in patients with lung cancer. China Tradit Chin Med Sci Technol 20: 115-116, 2013.
14. Yang FR, Zhao YF, Hu XW, Liu ZK, Yu XD, Li CY, Li XR and Li HJ: Nano-realgar suppresses lung cancer stem cell growth by repressing metabolic reprogramming. Gene 788: 145666, 2021.
15. Liu D, Zhi D, Zhou T, Yu Q, Wan F, Bai Y and Li H: Realgar bioleaching solution is a less toxic arsenic agent in suppressing the Ras/MAPK pathway in *Caenorhabditis elegans*. Environ Toxicol Pharmacol 35: 292-299, 2013.
16. Drosten M and Barbacid M: Targeting the MAPK Pathway in KRAS-driven tumors. Cancer Cell 37: 543-550, 2020.
17. Moore AR, Rosenberg SC, McCormick F and Malek S: RAS-targeted therapies: Is the undruggable drugged? Nat Rev Drug Discov 19: 533-552, 2020.
18. Karoulia Z, Gavathiotis E and Poulikakos PI: New perspectives for targeting RAF kinase in human cancer. Nat Rev Cancer 17: 676-691, 2017.
19. Karnoub AE and Weinberg RA: Ras oncogenes: Split personalities. Nat Rev Mol Cell Biol 9: 517-531, 2008.
20. Leevers SJ, Paterson HF and Marshall CJ: Requirement for Ras in Raf activation is overcome by targeting Raf to the plasma membrane. Nature 369: 411-414, 1994.
21. Stokoe D, Macdonald SG, Cadwallader K, Symons M and Hancock JF: Activation of Raf as a result of recruitment to the plasma membrane. Science 264: 1463-1467, 1994.
22. Peng SB, Henry JR, Kaufman MD, Lu WP, Smith BD, Vogeti S, Rutkoski TJ, Wise S, Chun L, Zhang Y, *et al*: Inhibition of RAF isoforms and active dimers by LY3009120 leads to anti-tumor activities in RAS or BRAF mutant cancers. Cancer Cell 28: 384-398, 2015.
23. Awad MM, Liu S, Rybkin II, Arbour KC, Dilly J, Zhu VW, Johnson ML, Heist RS, Patil T, Riely GJ, *et al*: Acquired resistance to KRAS^{G12C} inhibition in cancer. N Engl J Med 384: 2382-2393, 2021.
24. Tanaka N, Lin JJ, Li C, Ryan MB, Zhang J, Kiedrowski LA, Michel AG, Syed MU, Fella KA, Sakhi M, *et al*: Clinical acquired resistance to KRAS^{G12C} inhibition through a novel KRAS switch-II pocket mutation and polyclonal alterations converging on RAS-MAPK reactivation. Cancer Discov 11: 1913-1922, 2021.
25. Yagoda N, von Rechenberg M, Zaganjor E, Bauer AJ, Yang WS, Fridman DJ, Wolpaw AJ, Smukste I, Peltier JM, Boniface JJ, *et al*: RAS-RAF-MEK-dependent oxidative cell death involving voltage-dependent anion channels. Nature 447: 864-868, 2007.
26. Chen X, Kang R, Kroemer G and Tang D: Broadening horizons: The role of ferroptosis in cancer. Nat Rev Clin Oncol 18: 280-296, 2021.
27. Chen P, Li X, Zhang R, Liu S, Xiang Y, Zhang M, Chen X, Pan T, Yan L, Feng J, *et al*: Combinative treatment of β-elemene and cetuximab is sensitive to KRAS mutant colorectal cancer cells by inducing ferroptosis and inhibiting epithelial-mesenchymal transformation. Theranostics 10: 5107-5119, 2020.
28. Balihodzic A, Prinz F, Dengler MA, Calin GA, Jost PJ and Pichler M: Non-coding RNAs and ferroptosis: Potential implications for cancer therapy. Cell Death Differ 29: 1094-1106, 2022.
29. Alemán MR, Santolaria F, Batista N, de La Vega M, González-Reimers E, Milena A, Llanos M and Gómez-Sirvent JL: Leptin role in advanced lung cancer. A mediator of the acute phase response or a marker of the status of nutrition? Cytokine 19: 21-26, 2002.
30. Liang C, Zhang X, Yang M and Dong X: Recent progress in ferroptosis inducers for cancer therapy. Adv Mater 31: 1904197, 2019.
31. Gammella E, Buratti P, Cairo G and Recalcati S: The transferrin receptor: The cellular iron gate. Metallomics 9: 1367-1375, 2017.
32. Yang WS and Stockwell BR: Synthetic lethal screening identifies compounds activating iron-dependent, nonapoptotic cell death in oncogenic-RAS-harboring cancer cells. Chem Biol 15: 234-245, 2008.

33. Chen X, Yu C, Kang R, Kroemer G and Tang D: Cellular degradation systems in ferroptosis. Cell Death Differ 28: 1135-1148, 2021.
34. Deng S, Wu D, Li L, Liu T, Zhang T, Li J, Yu Y, He M, Zhao YY, Han R and Xu Y: miR-324-3p reverses cisplatin resistance by inducing GPX4-mediated ferroptosis in lung adenocarcinoma cell line A549. Biochem Biophys Res Commun 549: 54-60, 2021.
35. Kukulj S, Jaganjac M, Boranic M, Krizanac S, Santic Z and Poljak-Blazi M: Altered iron metabolism, inflammation, transferrin receptors, and ferritin expression in non-small-cell lung cancer. Med Oncol 27: 268-277, 2010.
36. Jaune-Pons E and Vasseur S: Role of amino acids in regulation of ROS balance in cancer. Arch Biochem Biophys 689: 108438, 2020.
37. Szklarczyk D, Gable AL, Nastou KC, Lyon D, Kirsch R, Pyysalo S, Doncheva NT, Legeay M, Fang T, Bork P, *et al*: The STRING database in 2021: Customizable protein-protein networks, and functional characterization of user-uploaded gene/measurement sets. Nucleic Acids Res 49 (D1): D605-D612, 2021.
38. Nie Q, Hu Y, Yu X, Li X and Fang X: Induction and application of ferroptosis in cancer therapy. Cancer Cell Int 22: 12, 2022.
39. Xu T, Ding W, Ji X, Ao X, Liu Y, Yu W and Wang J: Molecular mechanisms of ferroptosis and its role in cancer therapy. J Cell Mol Med 23: 4900-4912, 2019.
40. Sun L, Dong H, Zhang W, Wang N, Ni N, Bai X and Liu N: Lipid peroxidation, GSH depletion, and SLC7A11 inhibition are common causes of EMT and ferroptosis in A549 cells, but different in specific mechanisms. DNA Cell Biol 40: 172-183, 2021.
41. Wang H, Liu C, Zhao Y and Gao G: Mitochondria regulation in ferroptosis. Eur J Cell Biol 99: 151058, 2020.
42. Gao M, Yi J, Zhu J, Minikes AM, Monian P, Thompson CB and Jiang X: Role of mitochondria in ferroptosis. Mol Cell 73: 354-363.e3, 2019.
43. Yang WS, SriRamaratnam R, Welsch ME, Shimada K, Skouta R, Viswanathan VS, Cheah JH, Clemons PA, Shamji AF, Clish CB, *et al*: Regulation of ferroptotic cancer cell death by GPX4. Cell 156: 317-331, 2014.
44. Dixon SJ, Lemberg KM, Lamprecht MR, Skouta R, Zaitsev EM, Gleason CE, Patel DN, Bauer AJ, Cantley AM, Yang WS, *et al*: Ferroptosis: An iron-dependent form of nonapoptotic cell death. Cell 149: 1060-1072, 2012.
45. Doll S, Proneth B, Tyurina YY, Panzilius E, Kobayashi S, Ingold I, Irmler M, Beckers J, Aichler M, Walch A, *et al*: ACSL4 dictates ferroptosis sensitivity by shaping cellular lipid composition. Nat Chem Biol 13: 91-98, 2017.
46. Su LJ, Zhang JH, Gomez H, Murugan R, Hong X, Xu D, Jiang F and Peng ZY: Reactive oxygen species-induced lipid peroxidation in apoptosis, autophagy, and ferroptosis. Oxid Med Cell Longev 2019: 5080843, 2019.
47. Chang WT, Bow YD, Fu PJ, Li CY, Wu CY, Chang YH, Teng YN, Li RN, Lu MC, Liu YC and Chiu CC: A marine terpenoid, heteronemin, induces both the apoptosis and ferroptosis of hepatocellular carcinoma cells and involves the ROS and MAPK pathways. Oxid Med Cell Longev 2021: 7689045, 2021.
48. Zhao J and Luo Z: Discovery of Raf family is a milestone in deciphering the Ras-mediated intracellular signaling pathway. Int J Mol Sci 23: 5158, 2022.
49. Liu G, Song Y, Li C, Liu R, Chen Y, Yu L, Huang Q, Zhu D, Lu C, Yu X, *et al*: Arsenic compounds: The wide application and mechanisms applied in acute promyelocytic leukemia and carcinogenic toxicology. Eur J Med Chem 221: 113519, 2021.
50. Lin CC, Huang YK, Cho CF, Lin YS, Lo CC, Kuo TT, Tseng GC, Cheng WC, Chang WC, Hsiao TH, *et al*: Targeting positive feedback between BASP1 and EGFR as a therapeutic strategy for lung cancer progression. Theranostics 10: 10925-10939, 2020.
51. Cuenda A and Rousseau S: p38 MAP-kinases pathway regulation, function and role in human diseases. Biochim Biophys Acta 1773: 1358-1375, 2007.
52. Huang CH, Lee YC, Chiou JT, Shi YJ, Wang LJ and Chang LS: Arsenic trioxide-induced p38 MAPK and Akt mediated MCL1 downregulation causes apoptosis of BCR-ABL1-positive leukemia cells. Toxicol Appl Pharmacol 397: 115013, 2020 (Epub ahead of print).
53. Wu MF, Huang YH, Chiu LY, Cherng SH, Sheu GT and Yang TY: Curcumin induces apoptosis of chemoresistant lung cancer cells via ROS-regulated p38 MAPK phosphorylation. Int J Mol Sci 23: 8248, 2022.
54. Xiao X, Guo L, Dai W, Yan B, Zhang J, Yuan Q, Zhou L, Shan L and Efferth Y: Green tea-derived theabrownin suppresses human non-small cell lung carcinoma in xenograft model through activation of not only p53 signaling but also MAPK/JNK signaling pathway. J Ethnopharmacol 291: 115167, 2022.
55. Liu Z, Zhao M, Jiang X, Zhang Y, Zhang S, Xu Y, Ren H, Su H, Wang H and Qiu X: Upregulation of KLHL17 promotes the proliferation and migration of non-small cell lung cancer by activating the Ras/MAPK signaling pathway. Lab Invest: Aug 17, 2022 (Epub ahead of print).
56. Han YH, Moon HJ, You BR, Kim SZ, Kim SH and Park WH: The effect of MAPK inhibitors on arsenic trioxide-treated Calu-6 lung cells in relation to cell death, ROS and GSH levels. Anticancer Res 29: 3837-3844, 2009.
57. Yang X, Wu X, Wu X, Huang L, Song J, Yung C, He Z and Li Y: The flavagline compound 1-(2-(dimethylamino) acetyl)-rocaglaol induces apoptosis in K562 cells by regulating the PI3K/Akt/mTOR, JAK2/STAT3, and MAPK pathways. Drug Des Devel Ther 16: 2545-2557, 2022.
58. Lee H, Lee HJ, Bae IJ, Kim JJ and Kim SH: Inhibition of STAT3/VEGF/CDK2 axis signaling is critically involved in the antiangiogenic and apoptotic effects of arsenic herbal mixture PROS in non-small lung cancer cells. Oncotarget 8: 101771-101783, 2017.
59. Liu Z, Zhao Q, Zuo ZX, Yuan SQ, Yu K, Zhang Q, Zhang X, Sheng H, Ju HQ, Cheng H, *et al*: Systematic analysis of the aberrances and functional implications of ferroptosis in cancer. iScience 23: 101302, 2020.
60. Yong WP, Rha SY, Tan IB, Choo SP, Syn NL, Koh V, Tan SH, Asuncion BR, Sundar R, So JB, *et al*: Real-time tumor gene expression profiling to direct gastric cancer chemotherapy: Proof-of-concept '3G' trial. Clin Cancer Res 24: 5272-5281, 2018.
61. Jiang L, Kon N, Li T, Wang SJ, Su T, Hibshoosh H, Baer R and Gu W: Ferroptosis as a p53-mediated activity during tumour suppression. Nature 520: 57-62, 2015.
62. Lim JKM and Leprivier G: The impact of oncogenic RAS on redox balance and implications for cancer development. Cell Death Dis 10: 955, 2019.
63. Lim JKM, Delaidelli A, Minaker SW, Zhang HF, Colovic M, Yang H, Negri GL, von Karstedt S, Lockwood WW, Schaffer P, *et al*: Cystine/glutamate antiporter xCT (SLC7A11) facilitates oncogenic RAS transformation by preserving intracellular redox balance. Proc Natl Acad Sci USA 116: 9433-9442, 2019.
64. Baek S, Choi CM, Ahn SH, Lee JW, Gong G, Ryu JS, Oh SJ, Bacher-Stier C, Fels L, Koglin N, *et al*: Exploratory clinical trial of (4S)-4-(3-[18F]fluoropropyl)-L-glutamate for imaging xC-transporter using positron emission tomography in patients with non-small cell lung or breast cancer. Clin Cancer Res 18: 5427-5437, 2012.
65. Hu K, Li K, Lv J, Feng J, Chen J, Wu H, Cheng F, Jiang W, Wang J, Pei H, *et al*: Suppression of the SLC7A11/glutathione axis causes synthetic lethality in KRAS-mutant lung adenocarcinoma. J Clin Invest 130: 1752-1766, 2020.
66. Zhang N, Huang J, Xu M and Wang Y: LncRNA T-UCR Uc.339/miR-339/SLC7A11 axis regulates the metastasis of ferroptosis-induced lung adenocarcinoma. J Cancer 13: 1945-1957, 2022.
67. Liu XY, Wei DG and Li RS: Capsaicin induces ferroptosis of NSCLC by regulating SLC7A11/GPX4 signaling in vitro. Sci Rep 12: 11996, 2022.
68. Gao H, Bai Y, Jia Y, Zhao Y, Kang R, Tang D and Dai E: Ferroptosis is a lysosomal cell death process. Biochem Biophys Res Commun 503: 1550-1556, 2018.
69. Ma X, Yan W and He N: Lidocaine attenuates hypoxia/reoxygenation-induced inflammation, apoptosis and ferroptosis in lung epithelial cells by regulating the p38 MAPK pathway. Mol Med Rep 25: 150, 2022.
70. Yang J, Mo J, Dai J, Ye C, Cen W, Zheng X, Jiang L and Ye L: Cetuximab promotes RSL3-induced ferroptosis by suppressing the Nrf2/HO-1 signalling pathway in KRAS mutant colorectal cancer. Cell Death Dis 12: 1079, 2021.
71. Zhu K, Zhu X, Sun S, Yang W, Liu S, Tang Z, Zhang R, Li J, Shen T and Hei M: Inhibition of TLR4 prevents hippocampal hypoxic-ischemic injury by regulating ferroptosis in neonatal rats. Exp Neurol 345: 113828, 2021.
72. Wang Y, Zhang L, Yao C, Ma Y and Liu Y: Epithelial membrane protein 1 promotes sensitivity to RSL3-induced ferroptosis and intensifies gefitinib resistance in head and neck cancer. Oxid Med Cell Longev 2022: 4750671, 2022.